International Conference on Non-conventional Materials and Technologies
NOCMAT 2022

CO_2 RICH ENVIRONMENT AS A CURING METHOD FOR COMMERCIAL FIBRE-CEMENT CORRUGATED SHEETS

Carlos A. Fioroni, University of São Paulo, Brazil, carlosfioroni@usp.br
Gustavo H. D. Tonoli, University of Lavras, Brazil, gustavotonoli@yahoo.com.br
Rafael H. Filomeno, University of São Paulo, Brazil, rafaelfilomeno@usp.br
Zaqueu D. Freitas, University of São Paulo, Brazil, eng.zaqueu@gmail.com
Gustavo R. de Paula, Infibra S.A., Brazil, gustavorocha@infibra.com.br
Vanderley M. John, University of São Paulo, Brazil, vanderley.john@lme.pcc.usp.br
Holmer Savastano Jr., University of São Paulo, Brazil, holmersj@usp.br

ABSTRACT

This work presents a pilot-scale curing method based on accelerated carbonation. Commercial corrugated sheets, reinforced with cellulose and polypropylene fibres, produced by the Hatschek process were evaluated after the curing method in a CO_2 rich environment and compared with air-cured corrugated sheets. The curing was carried out in a chamber similar to an autoclave with 8 m^3 of internal volume especially designed for fibre-cement sheets curing. Three different manometric pressure conditions were tested: (I) sub-atmospheric (-0.5 bar); (II) atmospheric; (III) super-atmospheric (5 bar). The results for the three conditions were similar in several characteristics, standing out the super-atmospheric condition in some of them. Carbonation degrees of up to 38%, which means about 107 g of CO_2 incorporated per kg of dry composite, resulted in the increase of bulk density and the decrease of apparent porosity and water absorption. In terms of reinforcement, polypropylene fibres are challenging due to their low modulus of elasticity and poor fibre to matrix adhesion. The accelerated carbonation cured sheets showed a better fibre to matrix interface. The mechanical strength of the accelerated carbonation cured sheets increased by about 15%. The modulus of elasticity (6.3 GPa) and limit of proportionality (4.4 MPa) increased about 40% compared to air-cured sheets, leading to more rigid products. The dimensional stability evaluated by controlled drying shrinkage tests revealed dimensional variation around 1 mm/m in the accelerated carbonation cured sheets. The consumption of calcium hydroxide during the carbonation process at early ages of the composite, leading to lower matrix pH, is also a benefit that may decrease the cellulose fibre degradation under the alkaline environment. The benefits of the curing method also mitigated the defects by clogging the open pores and micro-fissures, providing higher physical-mechanical performance than the air-cured sheets. This curing method opens viable perspectives both for CO_2 capture in fibre-cement composites and polypropylene as reinforcement fibre for new technologies of fibre-cement.

KEYWORDS

Fibre-cement composites; Accelerated carbonation; CO_2 capture; Cellulose fibres; Polypropylene fibres.

INTRODUCTION

Fibre-cement is a composite whose matrix is made of Ordinary Portland Cement and mineral additions reinforced by synthetic and/or natural fibres. It is worldwide used in the manufacture of products such as flat boards for dry construction (steel-frame), ceilings, partitions and roofing elements (corrugated sheets) (Innocentini et al., 2019, 2022). Due to its relatively lower cost than other solutions, fibre-cement is considered a suitable material for use in various sectors of civil construction, primarily commercial segments, rural constructions and segments intended for the population with lower income (Savastano Júnior & Santos, 2008; Tonoli et al., 2011). The global fibre cement market is projected to grow from USD 16.4 billion in 2020 to USD 20.3 billion by 2025. The growing market can be attributed to the increase in demand for fibre cement products for construction activities, aided by the rise in government regulations on the use of asbestos across the globe. The high demand for environmentally friendly and sustainable construction products worldwide is also a reason for this market growing (Markets and Martkets, 2020).

Studies have demonstrated that the accelerated carbonation applied to fibre-cement composites on a laboratory scale increases the performance of the composite in several of its properties (Correia et al., 2015; Teixeira et al., 2014; Urrea-Ceferino et al., 2017). The exposition of fibre-cement to an atmosphere rich in CO_2 affords the gas diffusion through the matrix's unsaturated pores. The reaction of the carbonation of the hydration products of the Portland cement precipitate in form of calcium carbonate, causing both pores clogging and densification of the matrix. This effect decreases the composite porosity and permeable pores as well as the pores and voids in the interfacial zone between fibres and the matrix. Fibre to matrix interface is improved by better adhesion (Tonoli et al., 2009, 2019). Accelerated carbonation usually begins from the external layers of fibre-cement and gradually reaches the inner core. Different phases of $CaCO_3$ could be formed, such as vaterite, aragonite, and calcite, depending on the pressure and temperature conditions (Fioroni et al., 2020).

Several authors have achieved in their studies higher physical-mechanical performance and decreased the porosity of the fibre-cement produced in the laboratory. Carbonation degrees of around 44% increased nearly 30% of the mechanical properties (Tonoli et al., 2019). High degrees of carbonation (of 86%) reached in laboratory-scale commercial corrugated sheets curing revealed that properties directly related to the sheets' rigidity (LOP and MOE) could be double their values. The drying shrinkage was halved (reaching 1 mm/m) by the influence of laboratory-scale curing with accelerated carbonation which clogged pores with carbonates in the range of 0.06–1.50 mm (Fioroni et al., 2020).

This work has been motivated by the promising fibre-cement market and for the fact that accelerated carbonation could improve the performance of the fibre-cement. The objective of this work was to evaluate the performance of a pilot-scale curing method, including accelerated carbonation applied to commercial fibre-cement corrugated roofing sheets. Three different conditions in terms of pressure were used during the accelerated carbonation step: (I sub-atmospheric (-0.5 bar); II atmospheric; III super-atmospheric (5 bar)). The cured sheets with accelerated carbonation were compared with air-cured commercial fibre-cement corrugated sheets. The performance was evaluated by mechanical tests in small samples taken from the sheets and the full corrugated sheets. Physical properties and degree of carbonation were also assessed. Furthermore, scanning electron microscopy and dimensional stability (drying shrinkage) tests were used to understand the changes in the microstructure of the corrugated sheets and how the pilot-scale curing with accelerated carbonation influenced their performance.

MATERIALS AND METHODS

Corrugated sheets

Commercial corrugated sheets were provided by Infibra S.A., Brazil. The fibre-cement matrix used is essentially composed of Ordinary Portland Cement and limestone. The reinforcement is composed of cellulose fibres and polypropylene fibres. The sheets were produced by the industrial Hatschek process with four thin layers, which corresponds to a final nominal thickness of 5 mm, 920 mm in width, and 1220 mm in length. The initial curing was applied in a 50 m long tunnel at an average temperature of 65°C and a saturated environment (~100% RH) for approximately 8 h to assure enough strength to the sheets to be handled. After the demoulding, the sheets were sealed with polyethene film for saturation air curing until 8 days at room temperature (~25°C) and saturated environment (~100% RH). The moisture content present in the sheets at 8 days was (19.2 ± 1.4) %. A total of 650 corrugated sheets were used in these pilot-scale curing tests, corresponding to around 6,3 t. of dry fibre-cement composite.

Curing Methods

Saturated air curing

Some sheets were kept sealed with polyethene film to continue air curing until 15 days of age at room temperature (~25°C) and saturated environment (~100% RH). These air-cured sheets are considered in this work as control samples (Ctr.) These 15 days of curing also represent the average age the sheets usually wait in the stocks before being dispatched to the resellers or the end consumers.

Accelerated carbonation curing

After 8 days of initial curing (8 h tunnel + room temperature and saturated environment sealed with polyethene film), the sheets were submitted to accelerated carbonation inside a chamber especially designed for fibre-cement corrugated sheets curing, similar to an autoclave. Figure 1 shows the chamber with 200 sheets arranged on top of each other inside and prepared for starting the accelerated carbonation process. The autoclave used as a chamber is a Fhaizer, model FZR INDL/885-2017, Brazil, with a diameter of 1.6 m and an internal volume of 7.8 m^3. The accelerated carbonation parameters were adjusted to a temperature of 60°C and relative humidity of 60% and proceeded for 6 h. These parameters were chosen according to previous studies and the literature (Filomeno et al., 2020; Fioroni et al., 2020), which provided carbonation degrees of up to 86%. Before the CO_2 insertion, a pre-vacuum at -0.8 bar was applied for 15 min. to remove the excess air from the chamber and the composites' porous network. The concentration of CO_2 (supplied by Air Liquide, 100% of purity) inside the chamber was saturated (~100% vol.) through the constant insertion of the gas inside the chamber. Three different manometric pressure conditions during accelerated carbonation were tested: (I) sub-atmospheric (-0.5 bar); (II) atmospheric; (III) super-atmospheric (5 bar). A number of 200 corrugated sheets for each pressure condition were placed inside the chamber, which corresponds to 1,9 t. of dry fibre-cement composite. At the end of the accelerated carbonation, the sheets presented an average of (17,6 ± 1.0) % of moisture content. After the accelerated carbonation, the sheets were immersed in water for 5 min to rehydrate and proceed the curing sealed in polyethene film and left at room temperature (~25°C) and saturated environment until 15 days of age.

Figure 1 - The autoclave Fhaizer used as a chamber for accelerated carbonation, model FZR INDL/885-2017, Brazil. The diameter is 1.6 m, and the internal volume is 7.8 m³. 200 sheets were placed inside and prepared for the beginning of the accelerated carbonation process.

Thermogravimetry, carbonation degree and x-ray diffraction

In order to estimate the carbonation degree, samples of the sheets were immersed in isopropanol to stop hydration and then dried at 60°C (Zhang & Scherer, 2011). Samples were adequately crushed, sieved and prepared according to the methodology for thermogravimetric analysis (Scrivener et al., 2016). It is essential to highlight that all crushed material passed through the sieve to avoid losing any important phase. The analysis was performed in a Netzsch thermal analyser, STA449 F3, Germany, under an N_2 atmosphere with 50 mL/min. flow rate and heating rate of 10°C/min. until 1000°C. The amount of incorporated CO_2 was determined by the mass loss between 550°C and 1000°C, related to the carbonates, and then expressed on a non-volatile basis as a percentage (Tonoli et al., 2019). The carbonates already present in the fibre-cement were deducted, and the carbonation degree was determined according to Eq. 1 (Matsushita et al., 2000).

$$CD = \frac{(C - C_o)}{(C_{max} - C_o)} \times 100 \quad (1)$$

in which *CD* is the carbonation degree, C_{max} is the required CO_2 to react with the available oxides in the cement, then forming $CaCO_3$ retrieved from Eq. 2. *C* is the amount of CO_2 in the carbonated roofing sheets, and C_0 is the amount of CO_2 in non-carbonated sheets (Ctr.) (Huntzinger et al., 2009).

$$C_{max} = 0.785 \times (CaO - 0.56 \times Ca(CO_3) - 0.7 \times SO_3) + 1.091 \times MgO + 0.71 \times Na_2O + 0.468 \times K_2O \quad (2)$$

Eq. 2 presumes that the whole Na_2O, CaO, K_2O, and MgO formed in the matrix react with the CO_2, forming carbonates (Huntzinger et al., 2009). It excludes the amount of CaO combined as $CaCO_3$ and sulphates (Tonoli et al., 2019).

X-ray diffraction was applied to determine the hydration products and the $CaCO_3$ phases already present in the sheets and formed after accelerated carbonation. Samples were crushed into powder and sieved through 30 mesh (600 µm). All crushed material passed through the sieve. An X-ray diffractometer Rigaku Miniflex 600, Japan, with CuKα radiation generated at a voltage of 40 kV and a current of 30 mA was used to scan between 5–75° 2θ at 2°/min (Fioroni et al., 2020).

Microstructure, physical and mechanical characterisation

The microstructure of the sheets was examined through Scanning Electron Microscopy (SEM) performed by a FEI Quanta 660 FEG, USA and using backscattered electron detector mode (BSE) and acceleration voltage of 15 kV. Mounted samples were ground for 5 min on three different silicon carbide sandpaper (grit 220, 500 and 1200 in this order) lubricated with deodorised kerosene and then polished with diamond suspensions with the particle sizes of 6 μm (10 min.), 3 μm (20 min.) and 1 μm (30 min.) diluted in deodorised kerosene. The samples were then cleaned in an ultrasonic bath with isopropanol for 10 min. between each polishing step. Before SEM analysis, the mounted samples were carbon-coated using the Bal-Tec model SCD-050 (USA) metalliser (Fioroni et al., 2020).

Samples from the flat portions between crests and troughs of the sheets (flanks) were extracted by a water-cooled diamond circular saw. Water absorption, bulk density, and apparent porosity values were calculated from the average of 10 specimens for each condition. Physical properties were retrieved following procedures specified by ASTM C 948-81 Standards (ASTM C 948 - 81 Reapproved, 2016), and a statistical data processing of the values was performed with a 95% confidence interval.

Samples from the sheets flanks cut into (30 x 160 x 6) mm³ were used for mechanical assessment. The mechanical tests were performed in an Emic DL 30000 testing machine equipped with 1 kN load cell and four-point bending configuration to obtain the modulus of rupture (MOR) (Eq. 3), modulus of elasticity (MOE) (Eq. 4), the limit of proportionality (LOP) (Eq. 5) and specific energy (SE) (Eq. 6). LOP is described as the stress corresponding to the upper point of the stress-strain curve's linear (elastic) portion. SE is calculated as the work fulfilled during the bending test divided by the cross-sectional area of the tested samples. Integration of the area below the load-deflection curve to the point corresponding to a reduction of 90% of the maximum load was used to calculate the absorbed energy. Bending tests adopted a displacement rate of 5 mm/min. and a span of 135 mm (Fioroni et al., 2020; RILEM, 1984).

$$MOR = \frac{[3 \times P_{max} \times (L_{inf} - L_{sup})]}{2 \times w \times h^2} \quad (3)$$

$$MOE = \left[\frac{\left(276 \times L_{inf}^3\right)}{(1296 \times w \times h^3)}\right] \times \left(\frac{P}{\delta}\right) \quad (4)$$

$$LOP = \frac{[3 \times P_{lop} \times (L_{inf} - L_{sup})]}{2 \times w \times h^2} \quad (5)$$

$$SE = \left[\frac{1}{(h \times w)}\right] \times \int P(\delta) d\delta \quad (6)$$

in which, P_{max} is the maximum load, L_{inf} is the major span between the supports, L_{sup} is the minor span between the two loading points, w and h are the specimen width and depth, respectively. P is the load, and δ is the deformation. P_{lop} is the load at the upper point of the linear portion of the load versus deflection curve (Correia et al., 2015, 2018).

Additionally, mechanical tests were performed in full corrugated sheets (1220 mm long and 920 mm width). The tests were carried out in a universal testing machine, Time Group Inc., China, equipped with 20 kN load cell and three-point bending configuration. Bending tests adopted a displacement rate of 50 mm/min. The adopted spam was 1100 mm, and the load was applied with a loading pin of 230 mm width covering the whole sheet width as recommended by the (ABNT NBR 15210-2, 2019).

Dimensional stability (drying shrinkage)

The dimensional stability test was assessed from the sheets flanks cut into (30 x 160 x 6) mm³. The samples (never before dried, at 15 days of age) were first immersed in water for 24 h to become water-saturated. The tests begin by placing the samples in a chamber model EPL-4H, Espec, USA, at 23°C, 50% RH. The reference measurement is taken at the zero-day (beginning of the test) with the water-saturated samples. Daily measures assessed the changes in length due to controlled drying for 14 days. A dial gauge Mitutoyo, Japan, was used for the measurements, following the methodology found in the literature (Fioroni et al., 2020; Souza, 2014) and calculated by the Eq. 7.

$$DS = \frac{L_i - L_d}{L_i \times 1000} \quad (7)$$

in which *DS* is the drying shrinkage, L_i is the initial length of the sample (mm), L_d is the daily measurement of the sample (mm), the multiplier (1000) in the denominator is applied to give the result in mm/m.

RESULTS AND DISCUSSION

Thermogravimetry, carbonation degree and x-ray diffraction analysis

Figure 2 depicts the sheets' thermogravimetric and derivative weight curves from the three different accelerated carbonation curing conditions (Sub-atmospheric – Sub.; Atmospheric – Atm.; Super-atmospheric – Sup.) compared with air-cured sheets (control – Ctr.). It is observed that the three conditions have similar behaviour under heating until 1000°C. The weight loss in temperatures between 50 - 250°C is related to the decomposition of cement hydration products (Morandeau et al., 2014). The weight loss between 90 - 200°C is directly related to C-S-H, ettringite, monosulphoaluminate, monocarboaluminate (Frías & Goñi, 2013; Tonoli et al., 2019). The C-S-H is progressively converted into $CaCO_3$ and silica hydrates (S-H) due to its decalcification during the carbonation reaction (Bertos et al., 2004). A reduction of weight loss in the range of 100 - 350°C is observed in all different accelerated carbonation cured sheets (Sub., Atm. Sup.) compared with the air-cured sheets (Ctr.).

The weight loss peaks centralised at 470°C is related to the decomposition of $Ca(OH)_2$, which is more intense in the air-cured sheets (Ctr.). The minor loss of mass in the carbonated samples is explained by the fact that $Ca(OH)_2$ (C-H) is the main cement hydration product involved in the carbonation reaction. Nevertheless, residues of C-H may remain since they could be inaccessible while decalcification of C-S-H occurs (Tonoli et al., 2019).

The weight loss in the range between 500 - 950°C is related to the dissociation of the CO_2 from the carbonates during heating (Tonoli et al., 2019). A higher weight loss observed between 550 - 750°C for the three different accelerated carbonation cured sheets is related to the different polymorphs and poorly crystallised $CaCO_3$ (Villain et al., 2007). The most crystallised carbonates decompose at 750 – 950°C (Morandeau et al., 2014; Tonoli et al., 2019). In the peaks centralised at 790°C there is a higher weight loss for the three different accelerated carbonation cured sheets. The weight loss on the air-cured sheets is related to the limestone used in the formulation, which can also contain a certain amount of dolomite, which decomposes at 790°C. Weight losses at 750°C are explained by the presence of vaterite (Morandeau et al., 2014; Tonoli et al., 2019). Calcite and aragonite decompose at the same temperatures in the range of 680 – 950°C, depending on the crystallinity degree. Aragonite may occur in minor amounts because it requires higher temperatures than vaterite and calcite to precipitate during the carbonation process (Popescu et al., 2014; Tonoli et al., 2016).

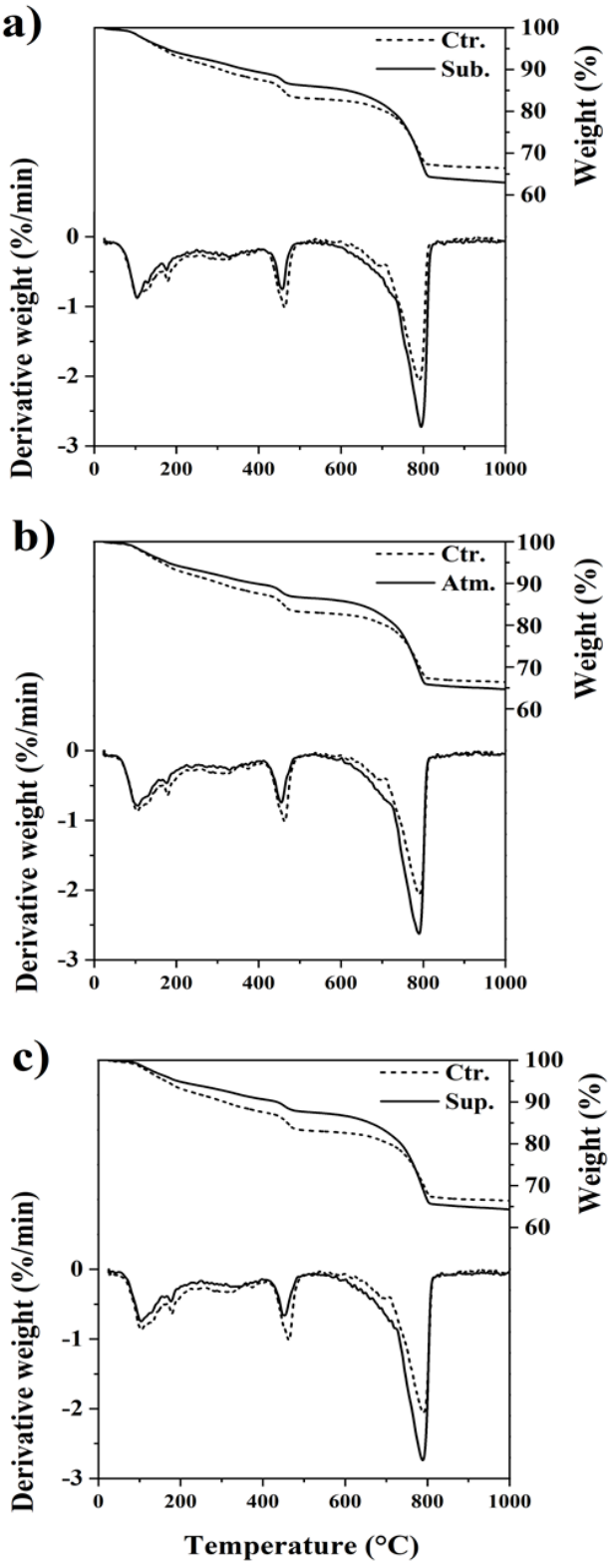

Figure 2 – Thermogravimetric and derivative weight curves for a) air-cured and accelerated carbonation cured sheets at sub-atmospheric pressure; b) air-cured and accelerated carbonation cured sheets at atmospheric pressure; c) air-cured and accelerated carbonation cured sheets at super-atmospheric pressure. Ctr. = air-cured sheets (control); Sub. = Accelerated carbonation cured sheets at sub-atmospheric pressure; Atm. = Accelerated carbonation cured sheets at atmospheric pressure; Sup. = Accelerated carbonation cured sheets at super-atmospheric pressure.

The carbonation degrees of the three different accelerated carbonation cured sheets are shown in Table 1. The carbonation degrees' values retrieved from the Eq.1 and Eq.2 were way close between the three different accelerated carbonation cured sheets, standing out the super-atmospheric condition. This fact can be explained by the high pressure (5 bar) that propitiates the chemical reactions evolved in the carbonation and force the CO_2 through the porous composite network. Sub-atmospheric pressure was also efficient because the excess of air was removed from the chamber and the pores of the composite. The CO_2 quickly penetrates the composite porous network and reacts with the carbonatable cement hydration products. The effectiveness of the atmospheric can be comparable with the other conditions. It is essential to highlight that before the insertion of CO_2 inside the chamber, a previous 15 min. under vacuum was carried out to take the excess air out from the chamber and the composite porous network, which improved the performance of the curing method.

According to the calculated carbonation degrees is possible to calculate the theoretical amount of CO_2 embodied in the sheets. The composite contains 65% of Portland Cement CPV-ARI (ABNT NBR 5733, equivalent to type III - ASTM C150 (AMERICAN SOCIETY FOR TESTING MATERIALS, 1981) or type V – BS EN-197-1), which admits a maximum of 15% of filler according to the Brazilian standards (in other words, is composed of 85% of clinker) which in turn is composed by 65% of CaO. In a ratio of 44/56 (CO_2/CaO) from molecular weight of $CaCO_3$, is possible to plot the graph (Figure 3) considering that 100% of carbonation degree would be the total amount of CO_2 necessary to combine with the whole CaO available in the composite. The chart in Figure 3 shows the trend of CO_2 incorporated by kg of composite according to the established conditions and parameters in this pilot-scale curing method. The amounts of embodied CO_2 provided by the pilot-scale accelerated carbonation curing were 104, 82 and 107 g for each kg of fibre-cement composite (or kg of corrugated sheets) for sub-atmospheric, atmospheric and super-atmospheric conditions, respectively. These values are pointed out in the graph in Figure 3. Thus, for the total amount of sheets placed inside the chamber in each pilot-scale test: sub-atmospheric accelerated carbonation incorporated about 202 kg of CO_2; atmospheric accelerated carbonation incorporated about 160 kg of CO_2; while the super-atmospheric accelerated carbonation incorporated about 208 kg of CO_2. These values are in line with those monitored during each test by the loss of masses of the CO_2 cylinders. These values show the potential of CO_2 capture by the composite while exposed to a rich CO_2 environment. Taking the super-atmospheric results as an example, the values can be extrapolated to the amount of CO_2 per covered area by the corrugated sheets (with a useful area of 0,94 m² at 9,7 kg (INFIBRA, 2020) and the numbers would be approximately 1,1 kg of CO_2 per square meter.

Table 1- Carbonation degrees retrieved from Eq.1 and Eq.2 for air-cured and accelerated carbonation cured corrugated sheets. Ctr. = air-cured sheets (control); Sub. = Accelerated carbonation cured sheets at sub-atmospheric pressure; Atm. = Accelerated carbonation cured sheets at atmospheric pressure; Sup. = Accelerated carbonation cured sheets at super-atmospheric pressure.

Corrugated Sheets	**Degree of carbonation (%)**
Ctr.	0
Sub.	37
Atm.	29
Sup.	38

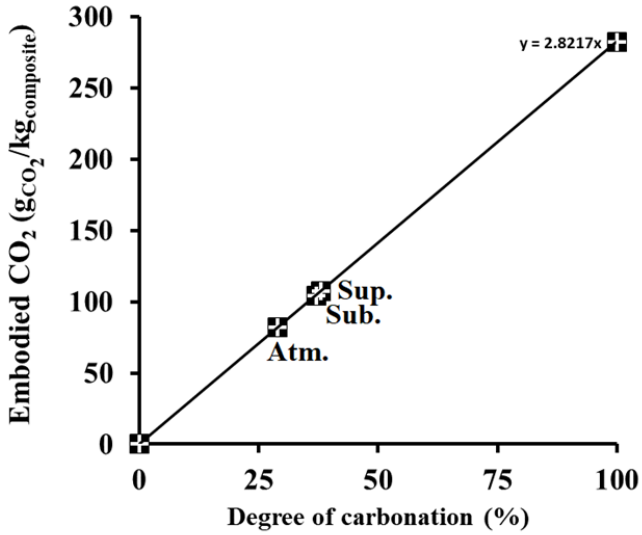

Figure 3 – Trend of embodied CO_2 given in grams of CO_2 per kg of composite. Sub. = Accelerated carbonation cured sheets at sub-atmospheric pressure; Atm. = Accelerated carbonation cured sheets at atmospheric pressure; Sup. = Accelerated carbonation cured sheets at super-atmospheric pressure.

The X-ray diffraction results are depicted in Figure 4. A noticeable reduction of $Ca(OH)_2$ was observed (peaks around 2θ = 18° and 34°) in all three different accelerated carbonation cured sheets (Sub., Atm. Sup.) when compared with air-cured sheets (Ctr.) (García-González et al., 2006; Kim et al., 2013). Due to pressure conditions and temperature, the reaction between $Ca(OH)_2$ and H_2CO_3 forms different phases of $CaCO_3$, such as vaterite, aragonite and calcite (Black et al., 2007; Hayakawa et al., 2008; Hunnicutt et al., 2017; Urrea-Ceferino et al., 2017). Besides that, CO_2 can react with other oxides forming other phases in small amounts (e.g. dolomite at 2θ = 31°). Accelerated carbonation cured sheets presented higher intensity peaks at 2θ = 29.5°, related to calcite phases (Hunnicutt et al., 2017; Santos et al., 2015). Other peaks at 2θ related to calcite appear in higher intensity in accelerated carbonation cured sheets. A peak around 2θ = 31° is related to dolomite, which comes from the dolomitic limestone used in the formulation and reactions of CO_2 and small amounts of MgO. Remnants of $Ca(OH)_2$ are also found in carbonated sheets in small quantities, corroborating with the results in thermogravimetric analysis that presented small weight loss at around 470°C Figure 2.

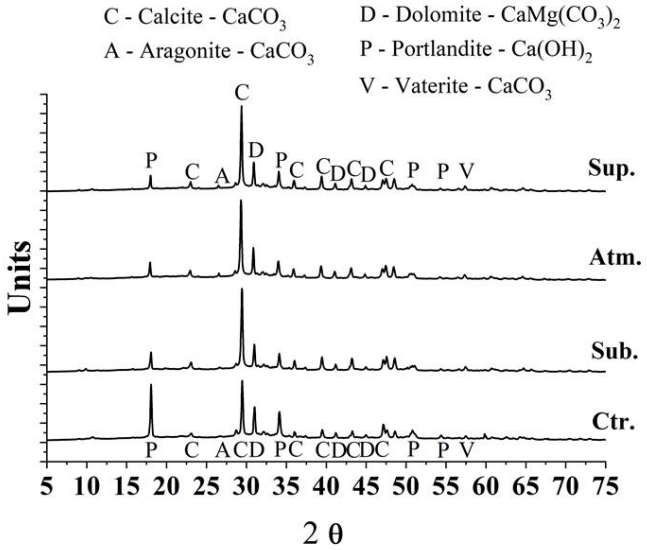

Figure 4 – X-ray diffractograms of the sheets. Ctr. = air-cured sheets (control); Sub. = Accelerated carbonation cured sheets at sub-atmospheric pressure; Atm. = Accelerated carbonation cured sheets at atmospheric pressure; Sup. = Accelerated carbonation cured sheets at super-atmospheric pressure.

Microstructure, physical and mechanical analysis

Figure 5 shows SEM images of a) air-cured sheet and b) accelerated carbonation cured sheet (Sup.) in polished surfaces samples. Due to their low atomic numbers, dark areas refer to cellulosic and polymeric fibres [26] and empty pores. Additionally, the accelerated carbonation cured sheet (Sup.) (Figure 4 b)) shows a clearer and smoother surface when compared with the air-cured sheet (Figure 4 a)). With the aid of a BSE detector, clearer regions were related to $CaCO_3$ (due to higher atomic numbers) formations in the voids of the cementitious matrix (Tonoli et al., 2016). Changes in the composites' microstructure are observed in the images, especially in terms of mitigation of porosity in the cementitious matrix and the fibre to matrix interface.

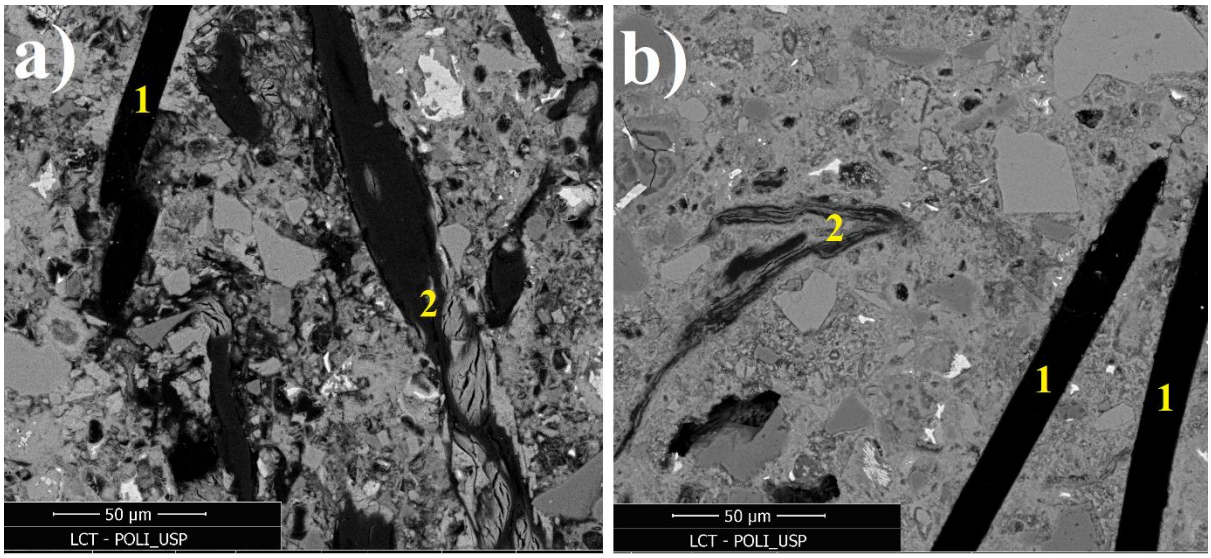

Figure 5 – Scanning electron micrographs: a) BSE image of air-cured sheet and b) BSE image of accelerated carbonation cured sheet at super-atmospheric pressure. Number 1 indicates polypropylene fibres and number 2 indicates cellulose fibres. In b) a clearer and smoother surface due to accelerated carbonation curing, indicating less porosity in the matrix. Image by Liz de Mello Zanchetta and adapted by the authors.

Table 2 shows the physical properties, while Figure 6 shows the sheets' bulk density chart. The accelerated carbonation increased the bulk density significantly and decreased water absorption and apparent porosity. The formation of $CaCO_3$, which is denser than $Ca(OH)_2$, fills the pores and voids and turns the matrix denser. The $CaCO_3$, which is denser and bulkier than $Ca(OH)_2$ and have a larger crystal size of $CaCO_3$ (aragonite - 227.34 $Å^3$, calcite - 367.65 $Å^3$) compared with $Ca(OH)_2$ (54.904 $Å^3$) (*Lafuente B., Downs R. T., Yang H., Stone N.*, 2015) directly contributes to the matrix densification. The sheets cured with super-atmospheric pressure during the accelerated carbonation stand out, showing 4% increase in bulk density value while the water absorption decreased by the same percentage. Apparent porosity was not significantly affected. As a result of the matrix modification by the accelerated carbonation, the performance of the sheets in terms of mechanical properties increased. Table 3 shows the mechanical properties of the sheets evaluated in their flanks (flat portions between crests and troughs).

Table 2 – Average and standard deviation values for physical properties of corrugated sheets. Ctr. = air-cured sheets (control); Sub. = Accelerated carbonation cured sheets at sub-atmospheric pressure; Atm. = Accelerated carbonation cured sheets at atmospheric pressure; Sup. = Accelerated carbonation cured sheets at super-atmospheric pressure. Capital letters (A, B and C) in the same column represent comparisons between conditions. Different letters indicate significant differences (Tukey, 5%, n = 10).

Corrugated Sheets	**Bulk Density (g/cm^3)**	**Apparent porosity (%)**	**Water absorption (%)**
Ctr.	1,38 ± 0.02 ^{A}	41.65 ± 0.69 ^{A}	30.24 ± 0.90 ^{A}
Sub.	1,41 ± 0.02 ^{B}	41.31 ± 1.00 ^{A}	29.30 ± 0.78 ^{AB}
Atm.	1,40 ± 0.02 ^{AB}	40.93 ± 1.27 ^{A}	29.20 ± 0.95 ^{B}
Sup.	1,44 ± 0.03 ^{C}	40.55 ± 0.66 ^{A}	28.15 ± 0.67 ^{C}

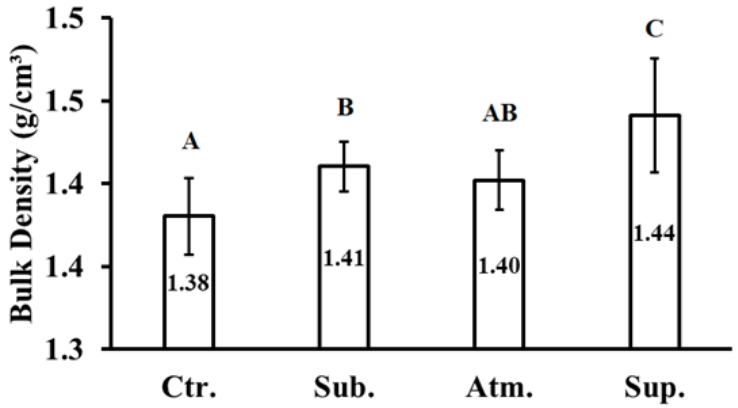

Figure 6 – Bulk density of the sheets: Ctr. = air-cured sheets (control); Sub. = Accelerated carbonation cured sheets at sub-atmospheric pressure; Atm. = Accelerated carbonation cured sheets at atmospheric pressure; Sup. = Accelerated carbonation cured sheets at super-atmospheric pressure. Capital letters (A, B and C) represent comparisons between conditions. Different letters indicate significant differences (Tukey, 5%, n = 10).

The mechanical properties of the sheets are shown in Table 3. In terms of mechanical properties, there are no significant differences between the three different accelerated carbonation cured sheets (Sub., Atm. Sup.). The mechanical strength (MOR) has increased by 13%, while the properties related to the stiffness (LOP and MOE) increased by 37% when compared to air-cured sheets (Ctr.). Higher values of specific energy (SE) were also observed. As a consequence of precipitation of $CaCO_3$, which fills the pores around the fibres and improves the anchoring of fibres to matrix, a decrease of the specific energy might be observed depending on the type of reinforcement (Filomeno et al., 2020). However, this is not the case in this work. Polypropylene is a hydrophobic fibre, and the association of accelerated carbonation in composites reinforced with polypropylene causes an improvement of fibre to matrix interface without losing the characteristic of pulling out of these fibres under stress. This effect absorbs energy and confers tenacity to the composite. Figure 7 shows the typical flexural stress-strain curves where a larger area is observed under the set of curves related to accelerated carbonation cured sheets. MOR is observed approximately at the same specific deformation as in air-cured sheets. There is no drawback in losing SE associated with the excess of fibre to matrix adhesion, the desired characteristic for these composites. On the other hand, the obtained results for the full corrugated sheets were slightly different.

Table 3 – Average and standard deviation values for mechanical properties determined on corrugated sheets' flanks (flat regions between crests and troughs). Ctr. = air-cured sheets (control); Sub. = Accelerated carbonation cured sheets at sub-atmospheric pressure; Atm. = Accelerated carbonation cured sheets at atmospheric pressure; Sup. = Accelerated carbonation cured sheets at super-atmospheric pressure. Capital letters (A and B) in the same column represent comparisons between conditions. Different letters indicate significant differences (Tukey, 5%, n = 10).

Corrugated Sheets' flanks	**MOR (MPa)**	**LOP (MPa)**	**MOE (GPa)**	**SE (kJ/m²)**
Ctr.	6.46 ± 0.48 ^{A}	3.03 ± 0.29 ^{A}	4.46 ± 0.63 ^{A}	6.74 ± 0.45 ^{A}
Sub.	7.32 ± 0.31 ^{B}	4,16 ± 0.47 ^{B}	6.13 ± 0.70 ^{B}	7.24 ± 0.41 ^{B}
Atm.	7.34 ± 0.41 ^{B}	4.26 ± 0.37 ^{B}	6.32 ± 0.82 ^{B}	7.47 ± 0.28 ^{B}
Sup.	7.46 ± 0.54 ^{B}	4.36 ± 0.31 ^{B}	6.30 ± 0.84 ^{B}	7.63 ± 0.42 ^{B}

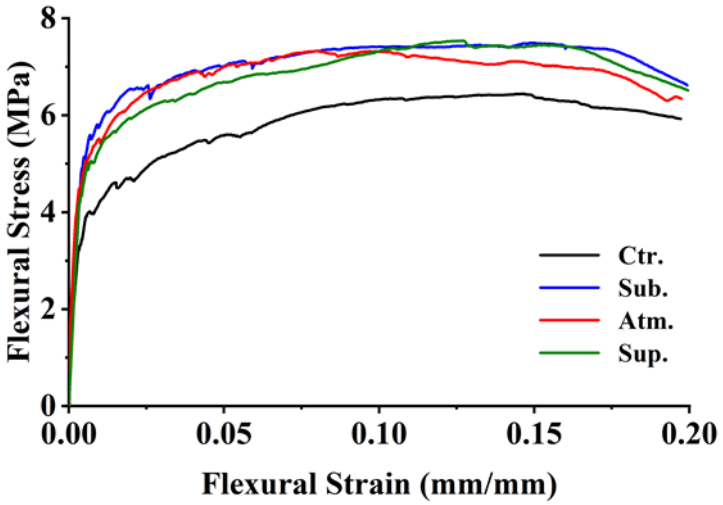

Figure 7 – Flexural Stress-strain typical curves of sheets' flanks (flat regions between crests and troughs): Ctr. = air-cured sheets (control); Sub. = Accelerated carbonation cured sheets at sub-atmospheric pressure; Atm. = Accelerated carbonation cured sheets at atmospheric pressure; Sup. = Accelerated carbonation cured sheets at super-atmospheric pressure.

The maximum loads supported by the sheets under mechanical tests are shown in Table 4, while the typical load-deformation curves are shown in Figure 8. There are significant differences between air-cured sheets and accelerated carbonation cured sheets, with a higher mechanical strength of around 20%. There are also significant differences between the sheets cured in different pressure conditions during the accelerated carbonation process. Sheets submitted under accelerated carbonation at atmospheric pressure presented lower results in terms of supported load (around 9 % in comparison to sub- and super-atmospheric).

Table 4 – Average and standard deviation values for maximum loads supported by the corrugated sheets. Ctr. = air-cured sheets (control); Sub. = Accelerated carbonation cured sheets at sub-atmospheric pressure; Atm. = Accelerated carbonation cured sheets at atmospheric pressure; Sup. = Accelerated carbonation cured sheets at super-atmospheric pressure. Capital letters (A, B and C) in the same column represent comparisons between conditions. Different letters indicate significant differences (Tukey, 5%, n = 5).

Corrugated Sheets	**Maximum load (kN/m)**
Ctr.	1.83 ± 0.05 ^{A}
Sub.	2.17 ± 0.09 ^{B}
Atm.	1.99 ± 0.04 ^{C}
Sup.	2.23 ± 0.06 ^{B}

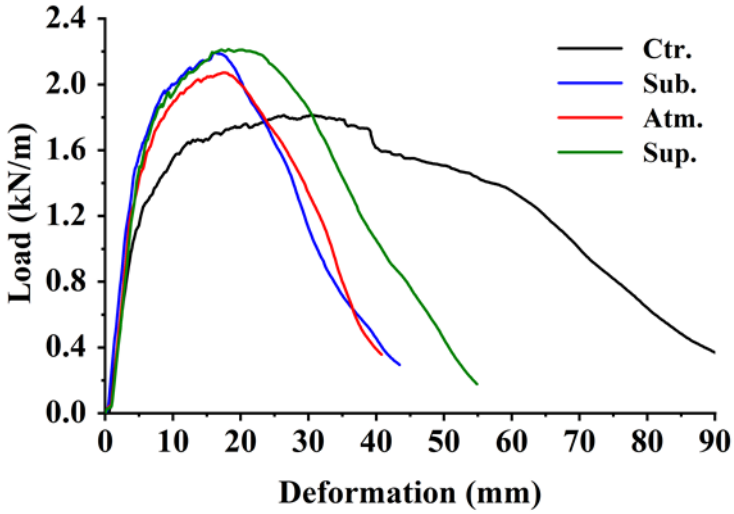

Figure 8 – Flexural Load-deformation typical curves of the sheets: Ctr. = air-cured sheets (control); Sub. = Accelerated carbonation cured sheets at sub-atmospheric pressure; Atm. = Accelerated carbonation cured sheets at atmospheric pressure; Sup. = Accelerated carbonation cured sheets at super-atmospheric pressure.

Drying shrinkage (dimensional stability) analysis

The physical tests evaluated an increase of density in the accelerated carbonation cured sheets, and according to the presented carbonation degrees of up to 38%, a decrease in drying shrinkage was also observed. The drying shrinkage (dimensional stability) results for air-cured and accelerated carbonation cured sheets with super-atmospheric are shown in Figure 9 a), while the moisture loss during the controlled drying is shown in Figure 9 b). The other accelerated carbonation conditions (sub-atmospheric and atmospheric) had similar behaviour to super-atmospheric, and both are omitted in the graph. There was a reduction from 1.75 mm/m (of air-cured sheets) to 1.00 mm/m (of super-atmospheric cured sheets) in samples after 14 days under controlled drying shrinkage. Expressive differences can already be noticed after 2 days of controlled drying. The mass loss (related to the moisture content of the samples) practically remained stabilised after 2 days for both sets of samples. The air-cured sheets samples (Ctr.) lost around 3.3 g of moisture while the super-atmospheric cured sheets samples lost less, about 3.0 g of moisture. It is explained by the less porosity of the carbonated composites, which absorb less moisture. According to authors (Fioroni et al., 2020; Souza, 2014), pores under 2.33 µm are subjected to great capillary stress, which causes great shrinkage of the composite due to the drying. By the precipitation of $CaCO_3$ into the porous network composite, this range of pores is clogged, then the capillary stress magnitude decreases by the less amount of active stress pores. Corrugated sheets cured on laboratory scale with accelerated carbonation showed less porosity in the range of 0.06 – 1.50 µm than their non-carbonated counterparts due to precipitation of $CaCO_3$ in this range of pores (Fioroni et al., 2020).

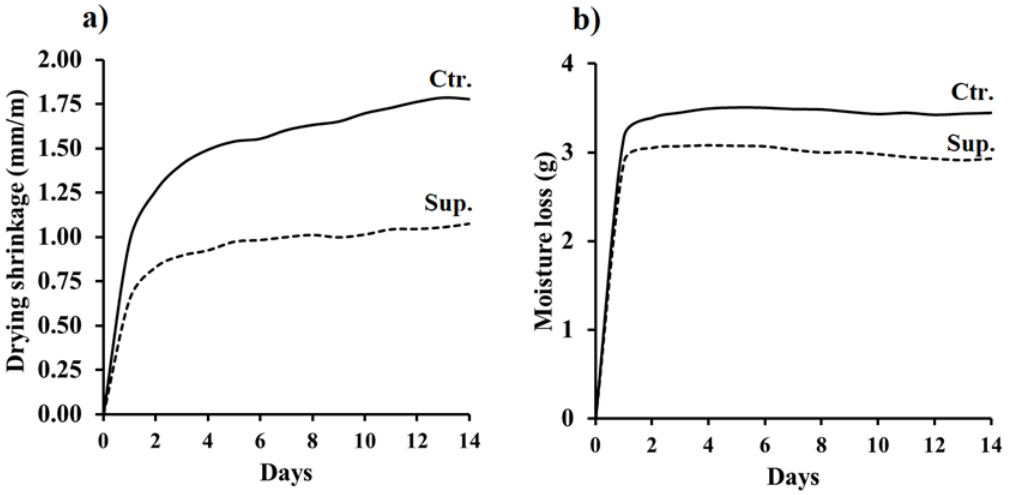

Figure 9 – a) Drying shrinkage (dimensional stability) results for air-cured corrugated sheets (Ctr.) and accelerated carbonation cured sheets by super-atmospheric pressure (Sup.). b) Moisture loss during the controlled drying at 23°C and 50% RH. Both parameters until 14 days.

CONCLUSIONS

The pilot-scale curing method, including accelerated carbonation, was an efficient method to improve the performance of fibre-cement corrugated sheets. Carbonation degrees of up to 38% were achieved with the method. The bulk density of the sheets increased (4%), and a decrease in water absorption was also observed. However, no significant reduction in apparent porosity was observed.

The curing method conferred better mechanical performance to the sheets, especially rigidity. The limit of proportionality (LOP) and the modulus of elasticity (MOE) increased by 37%, associated with the stiffening of the carbonated sheets. In an assessment of mechanical properties, not only in small samples but also in full corrugated sheets, the higher performance of the accelerated carbonation sheets could be observed at different manometric pressure (sub-atmospheric: -0.5 bar, atmospheric, super-atmospheric: 5 bar). Nevertheless, by the distribution of the load through the specific shape of the corrugated sheet, the behaviour observed by the load-deformation typical curves on the full sheets compared with the stress-strain curves on the small samples (from flanks) was slightly different. The stiffness behaviour could be well observed in the full sheets.

The formation of calcium carbonates was predominantly well crystallised in different phases such as aragonite, vaterite and calcite, the latter being predominant. The changes in microstructure and pore-clogging caused by the precipitation of $CaCO_3$ decreased considerably the drying shrinkage of accelerated carbonation cured sheets compared to air-cured sheets, achieving roughly 1 mm/m.

Cement-based corrugated sheets cured with accelerated carbonation have had a potential high performance compared to conventional air-cured cement-based corrugated sheets, especially in terms of mechanical performance and dimensional stability. The curing method also presented its potentiality in terms of capture of CO_2. The achieved carbonation degree (up to 38%) embodied up to 107 g of CO_2 per kg of fibre-cement composite. When converted on area basis, these values are up to 1,1 kg of CO_2 per square meter of roofing.

ACKNOWLEDGEMENTS

The authors would like to thank the São Paulo Research Foundation (FAPESP) grant n. 2015/50897-7, Infibra S.A., Leme/SP, Brazil and Imbralit Ltda., Crisciúma/SC, Brazil. This research was supported by: Embrapii PUSP-1903.0008, project nº CICS - nº 19.5.01; the National Institute of Science and Technology (INCT) - Advanced Eco-efficient Technologies in Cement Products (CEMtec) grant nº 88887.136401/2017-00-465593/2014-3; INCT grant nº 88887.159254/2017-00, São Paulo Research Foundation (FAPESP) grant n° 2014/50948-3. This work was carried out with the support of the Coordination for the Improvement of Higher Education Personnel (CAPES) - Brazil – "Financial Code 001". The authors also thank Mr Diego Ferrari (FZEA/USP), Ms Mariana Pavesi (FZEA/USP), Ms Liz de Mello Zanchetta (LME- POLI/USP).

CONFLICT OF INTEREST

The authors declare that they have no conflicts of interest associated with the work presented in this paper.

DATA AVAILABILITY

Data on which this paper is based is available from the authors upon reasonable request.

REFERENCES

ABNT NBR 15210-2:2019 Non-asbestos fibrecement corrugated sheets and their accessories Part 2 – Tests (In Portuguese), ABNT - Brazilian Association of Technical Standards. (2019).

AMERICAN SOCIETY FOR TESTING MATERIALS. (1981). ASTM C 150 - 81 Standard Specification for Portland Cement. In *Annual Book of ASTM Standards* (Issue Reapproved, p. 7).

ASTM C 948 - 81 Reapproved. (2016). *ASTM C 948 - 81 (Reapproved 2016) Standard test method for dry and wet bulk density, water absorption, and apparent porosity of thin sections of glass-fiber reinforced concrete*, *ASTM - American Society for Testing Materials*.

Bertos, M. F., Simons, S. J. R., Hills, C. D., & Carey, P. J. (2004). A review of accelerated carbonation technology in the treatment of cement-based materials and sequestration of CO_2. *Journal of Hazardous Materials*, *112*, 193–205. https://doi.org/10.1016/j.jhazmat.2004.04.019

Black, L., Breen, C., Yarwood, J., Garbev, K., Stemmermann, P., & Gasharova, B. (2007). Structural features of C-S-H(I) and its carbonation in air-A Raman spectroscopic study. Part II: Carbonated phases. *Journal of the American Ceramic Society*, *90*(3), 908–917. https://doi.org/10.1111/j.1551-2916.2006.01429.x

Correia, V. C., Santos, S. F., & Savastano Júnior, H. (2015). Effect of the accelerated carbonation in fibercement composites reinforced with eucalyptus pulp and nanofibrillated cellulose. *Materials and Matallurgical Engineering*, *9*(1), 7–10.

Correia, V. C., Santos, S. F., Teixeira, R. S., & Savastano Júnior, H. (2018). Nanofibrillated cellulose and cellulosic pulp for reinforcement of the extruded cement based materials. *Construction and Building Materials*, *160*, 376–384. https://doi.org/10.1016/j.conbuildmat.2017.11.066

Filomeno, R. H., Rodier, L. B., Ballesteros, J. E. M., Rossignolo, J. A., & Savastano, H. (2020). Optimizing the modified atmosphere parameters in the carbonation process for improved fiber-cement performance. *Journal of Building Engineering*. https://doi.org/10.1016/j.jobe.2020.101676

Fioroni, C. A., Innocentini, M. D. M., de Los Dolores, G. M., Tonoli, G. H. D., de Paula, G. R., & Savastano Júnior, H. (2020). Cement-based corrugated sheets reinforced with polypropylene fibres subjected to a high-performance curing method. *Construction and Building Materials*, *262*. https://doi.org/10.1016/j.conbuildmat.2020.120791

Frías, M., & Goñi, S. (2013). Accelerated carbonation effect on behaviour of ternary Portland cements. *Composites Part B: Engineering*, *48*, 122–128. https://doi.org/10.1016/j.compositesb.2012.12.008

García-González, C. A., Hidalgo, A., Andrade, C., Alonso, M. C., Fraile, J., López-Periago, A. M., & Domingo, C. (2006). Modification of composition and microstructure of Portland cement pastes as a result of natural and supercritical carbonation procedures. *Industrial and Engineering Chemistry Research*, *45*(14), 4985–4992. https://doi.org/10.1021/ie0603363

Hayakawa, S., Hajima, Y., Qiao, S., Namatame, H., & Hirokawa, T. (2008). Characterization of calcium carbonate polymorphs with Ca K edge X-ray absorption fine structure spectroscopy. *Analytical Sciences*, *24*, 835–837. https://doi.org/10.2116/analsci.24.835

Hunnicutt, W., Struble, L., & Mondal, P. (2017). Effect of synthesis procedure on carbonation of calcium-silicate-hydrate. *Journal of the American Ceramic Society*, *100*, 3736–3745. https://doi.org/10.1111/jace.14899

Huntzinger, D. N., Gierke, J. S., Kawatra, S. K., Eisele, T. C., & Sutter, L. L. (2009). Carbon dioxide sequestration in cement kiln dust through mineral carbonation. *Environmental Science & Technology*, *43*, 1986–1992. http://www.ncbi.nlm.nih.gov/pubmed/19368202

INFIBRA roof tile handling and assembly manual. In Portuguese: Manual de manuseio e montagem de telhas INFIBRA. (2020). https://infibra.com.br/wp-content/uploads/2017/09/Manual_telhas.pdf

Innocentini, M. D. M., Araújo Neto, O., & Crespi, M. R. (2022). Rapid non-destructive evaluation of the air and water permeability of commercial corrugated fibercement roofing sheets. *Construction and Building Materials*, *322*(January), 126457. https://doi.org/10.1016/j.conbuildmat.2022.126457

Innocentini, M. D. M., Faria, M. A. V., Crespi, M. R., & Andrade, V. H. B. (2019). Air permeability assessment of corrugated fiber-cement roofing sheets. *Cement and Concrete Composites*, *97*, 259–267. https://doi.org/10.1016/j.cemconcomp.2019.01.004

Kim, M. S., Jun, Y., Lee, C., & Oh, J. E. (2013). Use of CaO as an activator for producing a price-competitive non-cement structural binder using ground granulated blast furnace slag. *Cement and Concrete Research*, *54*, 208–214. https://doi.org/10.1016/j.cemconres.2013.09.011

Lafuente B., Downs R. T., Yang H., Stone N. (2015) The power of databases: the RRUFF project. In: Highlights in Mineralogical Crystallography, T. Armbruster and R. M. Danisi, eds. Berlin, Germany, W. De Gruyter, pp 1-30. (2015).

Markets and Martkets. (2020). Fiber Cement Market. https://www.marketsandmarkets.com/Market-Reports/fiber-cement-market-186027265.html

Matsushita, F., Aono, Y., & Shibata, S. (2000). Carbonation degree of autoclaved aerated concrete. *Cement and Concrete Research*, *30*, 1741–1745. https://doi.org/10.1016/S0008-8846(00)00424-5

Morandeau, A., Thiéry, M., & Dangla, P. (2014). Investigation of the carbonation mechanism of CH and C-S-H in terms of kinetics, microstructure changes and moisture properties. *Cement and Concrete Research*, *56*, 153–170. https://doi.org/10.1016/j.cemconres.2013.11.015

Popescu, M. A., Isopescu, R., Matei, C., Fagarasan, G., & Plesu, V. (2014). Thermal decomposition of calcium carbonate polymorphs precipitated in the presence of ammonia and alkylamines. *Advanced Powder Technology*, *25*, 500–507. https://doi.org/10.1016/j.apt.2013.08.003

RILEM. (1984). Reunion Internationale des Laboratooires d'essais et des Recheches sur les Materiaux et les Constructions. RILEM Technical Committee 49TFR: Testing methods for fibre reinforced cement-based composites. *Materiaux et Constructions*, *17*(102), 441–456.

Santos, S. F., Fiorelli, J., & Savastano Júnior, H. (2015). Non-conventional cement-based composites reinforced with vegetable. *Materiales de Construción*, *65*(317), 1–19.

Savastano Júnior, H., & Santos, S. F. (2008). Uso de resíduos de fibra vegetal em construção. *Com Ciência: Revista Eletrônica de Jornalismo Científico*. http://www.comciencia.br/comciencia/handler.php?section=8&edicao=32&id=382

Scrivener, K. L., Snellings, R., & Lothenbach, B. (2016). *A practical guide to microstructural analysis of cementitious materials* (C. P. T. & F. Group (Ed.); 1st ed.).

Souza, R. B. (2014). *Study of drying shrinkage in fiber- cement reinforced with polimeric fibre. 244 p. PhD Thesis, (in Portuguese)* [University of São Paulo]. https://doi.org/10.11606/T.3.2013.tde-22102014-095743

Teixeira, R. S., Tonoli, G. H. D., Santos, S. F., Savastano Júnior, H., Protásio, T. P., Toro, E. F., Maldonado, J., Lahr, F. A. R., & Delvasto, S. (2014). Different ageing conditions on cementitious roofing tiles reinforced with alternative vegetable and synthetic fibres. *Material and Structures*, *47*, 433–446. https://doi.org/10.1617/s11527-013-0070-0

Tonoli, G. H. D., Carmello, G. F., Fioroni, C. A., Pereira, T. D. L., Rocha, G., Souza, R. B. D., John, V. M., & Savastano Júnior, H. (2019). Influence of the initial moisture content on the carbonation degree and performance of fiber-cement composites. *Construction and Building Materials*, *215*(Special Issue), 22–29. https://doi.org/10.1016/j.conbuildmat.2019.04.159

Tonoli, G. H. D., Pizzol, V. D., Urrea, G., Santos, S. F., Mendes, L. M., Santos, V., John, V. M., Frías, M., & Savastano Júnior, H. (2016). Rationalizing the impact of aging on fiber–matrix interface and stability of cement-based composites submitted to carbonation at early ages. *Journal of Materials Science*, *51*, 7929–7943. https://doi.org/10.1007/s10853-016-0060-z

Tonoli, G. H. D., Rodrigues Filho, U. P., Savastano Júnior, H., Bras, J., Belgacem, M. N., & Lahr, F. A. R. (2009). Cellulose modified fibres in cement based composites. *Composites Part A: Applied Science and Manufacturing*, *40*, 2046–2053. https://doi.org/10.1016/j.compositesa.2009.09.016

Tonoli, G. H. D., Santos, S. F., Savastano Júnior, H., Delvasto, S., Gutiérrez, R. M., & Murphy, M. M. L. (2011). Effects of natural weathering on microstructure and mineral composition of cementitious roofing tiles reinforced with fique fibre. *Cement and Concrete Composites*, *33*(2), 225–232. https://doi.org/10.1016/j.cemconcomp.2010.10.013

Urrea-Ceferino, G. E., Rempe, N., Santos, V., & Savastano Júnior, H. (2017). Definition of optimal parameters for supercritical carbonation treatment of vegetable fiber-cement composites at a very early age. *Construction and Building Materials*, *152*, 424–433. https://doi.org/10.1016/j.conbuildmat.2017.06.182

Villain, G., Thiery, M., & Platret, G. (2007). Measurement methods of carbonation profiles in concrete: Thermogravimetry, chemical analysis and gammadensimetry. *Cement and Concrete Research*, *37*(8), 1182–1192. https://doi.org/10.1016/j.cemconres.2007.04.015

Zhang, J., & Scherer, G. W. (2011). Comparison of methods for arresting hydration of cement. *Cement and Concrete Research*, *41*, 1024–1036. https://doi.org/10.1016/j.cemconres.2011.06.003